EFFECT OF THE BOUNDARIES OF CRYSTALLINE GRAINS OF A SPECIAL GEOMETRY ON THE KINETICS OF RECRYSTALLIZATION AND GROWTH OF GRAINS

N.L. VASILIEV, S.V. SHEVCHENKO, S.L. SEMIATIN [1]

UDC 004.94:519.245:548.53

Institute for Metal Physics, Nat. Acad. Sci. of Ukraine
(36, Academician Vernadsky Str., Kyiv 03142, Ukraine; e-mail: shevchsv@imp.kiev.ua),

Air Force Research Laboratory, Materials and Manufacturing Directorate
(Wright-Patterson Air Force Base, OH 45433, USA)

The objective of the present work was to determine how the properties of grain boundaries (GB) of the coincidence-site-lattice (CSL) type affect the recrystallization and the grain growth kinetics. Traditionally, simple dependences of the GB energy and mobility on a scalar misorientation have been used in computer simulations; i.e. the low-angle boundaries (LABs) and the high-angle boundaries (HABs) have been assumed to exhibit low and high effective mobilities (EMs), respectively. To overcome the shortcomings associated with such an approach, the kinetics of recrystallization in the case where the EM of near-CSL boundaries deviates measurably from that of general HABs is examined using a 3D Monte-Carlo (MC) technique. A special model approach is developed to incorporate realistic starting conditions (microstructure, texture) and simulation parameters (the GB EM and a spatial distribution of stored energy).

1. Introduction

Many metallic structural materials are produced commercially via the thermomechanical processing of large ingots with starting coarse grain size. The conversion of such ingots to obtain a fine recrystallized microstructure usually relies on recrystallization, sometimes followed by the grain growth. Because these processes control the microstructure evolution, they are critical to the optimization of a subsequent fabrication or service properties. In particular, the static recrystallization often controls the post-processing grain size and texture in deformed-and-heat-treated materials. Hence, the phenomenology and the mechanisms of recrystallization have been studied extensively over the past several decades. This research and the latest developments in this subject are summarized in [1–3].

Recently, substantial progress in the understanding of recrystallization phenomena has been achieved by using various analytical and numerical model approaches [4–11]. As a result, a qualitative, and sometimes quantitative, description of the evolution of a microstructure and a texture during recrystallization has been developed in [3, 12]. Moreover, it has become increasingly recognized that these processes of evolution of the microstructure and the texture are closely related [13, 14] and should be taken into account in the development of advanced modeling routines [15, 16].

In many cases, nearly random textures are produced after only a moderate deformation. On the other hand, annealing after very heavy reductions can lead to the appearance of a strong texture during recrystallization. There are two major alternative explanations for the formation of such a texture – namely "oriented nucleation" and "oriented growth". Both theories postulate that a group of new recrystallized grains exhibits a special behavior and thereby dominates during the recrystallization process. For example, it is a common observation that the grains with boundaries close to $\Sigma 7$ orientation in fcc metals and $\Sigma 9$ or $\Sigma 19a$ in bcc materials grow much faster than randomly misoriented grains [2, 3].

Motivated by recent efforts, the objective of the present work was, therefore, to determine how the properties of grain boundaries of the CSL type affect the recrystallization and the grain growth kinetics.

Based on a 3D Monte-Carlo (Potts) approach, the present model incorporates the complete description of a microstructure and a texture and takes into account both the recrystallization driven by a stored energy and the thermally activated grain-boundary migration [17]. As a result, the simultaneous simulation of the recrystallization and the grain growth became possible.

2. Monte-Carlo Model for the Recrystallization and the Grain Growth

The grain growth within a recrystallized volume does not affect the recrystallized-fraction kinetics, but can have a significant effect on the texture and the microstructure of a final material. Hence, the recrystallization in the current work is treated in the typical manner as a process comprising the nucleation and the growth of new (recrystallized) grains; simultaneously, the thermally activated migration of all other GBs (within both the recrystallized and unrecrystallized volumes) was taken into account.

2.1. Initial texture and grain structure for MC simulations

The MC model domain (MD) was formed as a 3D cubic array of model units (MUs), each of which represented a point in the cubic lattice. The evolution of a microstructure and a texture within the model domain was simulated as in the previous work utilizing the MC approach to describe the interaction of grain growth and texture evolution [15,16]. In all calculations, the length of the side of the MD was set equal to 250 MUs; hence, the model domain was large enough (15,625,000 MUs) to obtain an adequate statistical representation of the microstructure and the texture.

To define the grain orientation with respect to the specimen (or the model domain) axes, three Euler angles (φ_1, Φ, and φ_2 in the Bunge notation [18, 19]) were used. Specific values of the stored energy ΔH and the crystallographic orientation $g = \{\varphi_1, \Phi, \varphi_2\}$ ($0 \leq \varphi_1 < 360$, $0 \leq \Phi < 90$, $0 \leq \varphi_2 < 90$) were associated with each MU. Each grain was characterized by a volume equal to the number of MUs that comprised it.

A special procedure was developed to create the initial textural state in the model domain and thus to replicate the specified orientation-distribution function (ODF) as closely as possible. This procedure was based on the following probabilistic function:

$$P(\Omega_j) = \frac{1}{V_{MD}} \frac{1}{N_g(\Omega_j)} \sum_{MD} V(G_i)\, \chi(g(G_i)),$$
$$\chi(g(G_i)) = \begin{cases} 1, & g(G_i) \in \Omega_j, \\ 0, & g(G_i) \notin \Omega_j, \end{cases} \quad (1)$$

in which $g(G_i)$ is the orientation of the i-th MU, $V(G_i)$ is the number of MUs oriented as $g(G_i)$, N_g is the total number of orientations g within the volume Ω_j, and V_{MD} is the volume of the overall model domain. From tests on model textures, it was determined that this procedure gave very good results when there were 100 or more grains.

A stochastic procedure was developed to create the initial microstructure in the model domain and to replicate experimentally observed microstructures with specific deformed-grain aspect. For this purpose, the number of grains within the model domain was determined first from the average grain size. Then, a corresponding number of MU locations was selected at random, at which the grains were to be created in the model volume. The remaining MUs were then assigned to these initial grains in a probabilistic manner.

2.2. Grain-boundary misorientation in the MC simulations

The single parameter consisting of the lattice misorientation between neighboring grains was used to define the relative grain-boundary energy and mobility. Therefore, the present modeling routine used the (approximate) scalar misorientation ε between grains having orientations $g_1$and g_2 [20], i.e.,

$$\varepsilon = \arccos\left(\frac{m_{11} + m_{22} + m_{33} - 1}{2}\right), \quad (2)$$

in which the elements m_{ij} form the matrix

$$\mathbf{M} = \mathbf{M}_{g_1} \times \mathbf{M}_{g_2}^{-1} = \begin{pmatrix} m_{11} & m_{12} & m_{13} \\ m_{21} & m_{22} & m_{23} \\ m_{31} & m_{32} & m_{33} \end{pmatrix}, \quad (3)$$

and the rotation matrices $\mathbf{M}_{g_1}$, $\mathbf{M}_{g_2}$correspond to orientations g_1 and g_2 [21,22].

The evaluation of the scalar misorientation would require much time if done for each MC trial, even using effective calculation schemes such as that based on quaternions [23]. Therefore, a database of ε as a discrete function of g_1 and g_2 was calculated and loaded into the computer memory prior to modeling. Thus, only a single search operation was performed for each MC trial.

2.3. Grain-boundary energy and mobility

The existing experimental data for the dependence of the grain-boundary energy and the mobility on the local lattice misorientation ε are sparse [24–29]. Even with the results collected in [27], it is not possible to fully describe the grain-boundary energy and the mobility as functions of the exact grain-boundary misorientation. Nevertheless, from a qualitative perspective, all of the measurements are similar to those shown in Fig. 1,*a* for the boundary energy and the mobility as a function of the scalar misorientation. Thus, LABs and HABs were assumed to exhibit low and high EM, respectively. However, as mentioned in Section 1, some CSL-type grain boundaries exhibit special properties and thus markedly affect the recrystallization. Specific values of the EM for CSL boundaries are discussed in Section 3 below.

2.4. Grain-boundary migration in the MC model

To simulate the kinetics of boundary motion with the MC technique, an MU site was selected at random. Each MU was characterized by its set of Euler angles and a ΔH value. If $\Delta H{>}0$, the MU was assumed to belong to the unrecrystallized volume. A possible new MU orientation was then randomly selected from the orientations of the adjacent grains (i.e. adjacent MUs with orientations that differ from the orientation of the current MU). If the MU belonged to the recrystallization front and was already denoted as recrystallized, the new-orientation selection was restricted to orientations of the adjacent recrystallized grains. This was followed by a re-orientation attempt according to a typical MC trial procedure [15, 16]. The local grain-boundary velocity is thus fully determined by local conditions. Hence, the energy minimization for the entire model domain is equivalent to the energy minimization in the local area Ω_{Sj} close to the MU:

$$E_L = \frac{1}{2}\sum_{j=1}^{\Omega_n}\left(1-\delta_{S_iS_j}\right)+H_i, \tag{4}$$

in which Ω_n denotes the number of MUs in the local area around the S_i model unit, and H_i is the stored energy associated with the model unit S_i.

The probability of the re-orientation of the S_i model unit from state g_k to state g_l is

$$P=\begin{cases} M_E(\varepsilon)\exp\left(\frac{-\Delta E_L}{k_bT_l}\right), & \Delta E_L>0,\\ M_E(\varepsilon), & \Delta E_L\le 0; \end{cases}$$

$$\Delta E_L = E_L(g_l)-E_L(g_k), \quad \varepsilon=\varepsilon(g_k,g_l), \tag{5}$$

or, when an MU belongs to the recrystallization front and not yet denoted as recrystallized,

$$P = U(\varepsilon)\frac{\Delta H\,(\varepsilon)}{\Delta H_{\mathrm{MAX}}}F\left(\Omega_{S_i}\right)\exp\left(\frac{-\Delta E_L}{k_bT_l}\right), \tag{6}$$

in which $F\left(\Omega_{S_i}\right)$ is the local shape factor for the MUs that belong to the recrystallization front. The grain-boundary energy in most cases is 2 to 3 orders of magnitude *less* than the average stored energy ΔH [27] and thus neglected in Eq. (6). The factor $F\left(\Omega_{S_i}\right)$ represents the effect of the difference in the coordination numbers of neighboring MUs on the flip probability for the current MC trial. The quantity T_l in Eqs. (5) and (6) denotes the "model lattice temperature" introduced into MC simulations to overcome lattice-pinning effects.

3. MC Model Results

The recrystallization kinetics for cases in which the EM of near-CSL boundaries deviates measurably from that of general HABs was examined to clarify the influence of such boundaries on the overall behavior. Specifically, the attention was focused on three cases. In each instance, the model domain had a sharp, *single-component* initial texture; and the oriented continuous nucleation of recrystallized grains was assumed [2, 3]. Furthermore, it was assumed that grain boundaries were preferred sites for the nucleation of recrystallized grains, and the recrystallization nuclei had a special boundary of the $\Sigma7$ or $\Sigma9$ type or a general HAB with one of the adjacent grains. The initial microstructure was assumed to comprise grains with a volume of 8000 MU^3 and the aspect ratio of 5:1:1.

The nucleation rate for each MCS within the unrecrystallized material was set, by assuming a constant nucleation rate of 10^{-4} nuclei/ MU^3. The recrystallization nuclei were assumed to be equiaxed (i.e., have the aspect ratio of 1:1:1) with an average volume of 15 MU^3.

3.1. Case 1 and 2

For two of the MC simulations, it was assumed that EM of CSL-type grain boundaries was about 43% *higher* (Case 1) or 50% *lower* (Case 2) than the EM of general HABs (Fig. 1,*b*). Typically, the precise description of the properties of special boundaries is possible only by using the effective mobility as a function of the *exact*

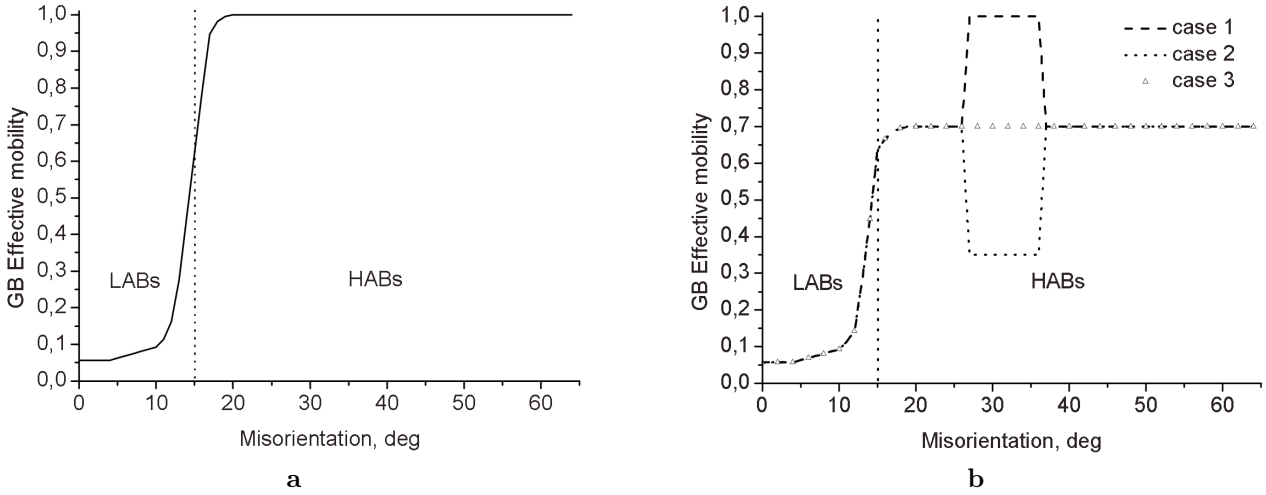

Fig. 1. Dependence of grain-boundary effective mobility on scalar misorientation: (*a*) general measurements and (*b*) assumed behavior for Cases 1–3

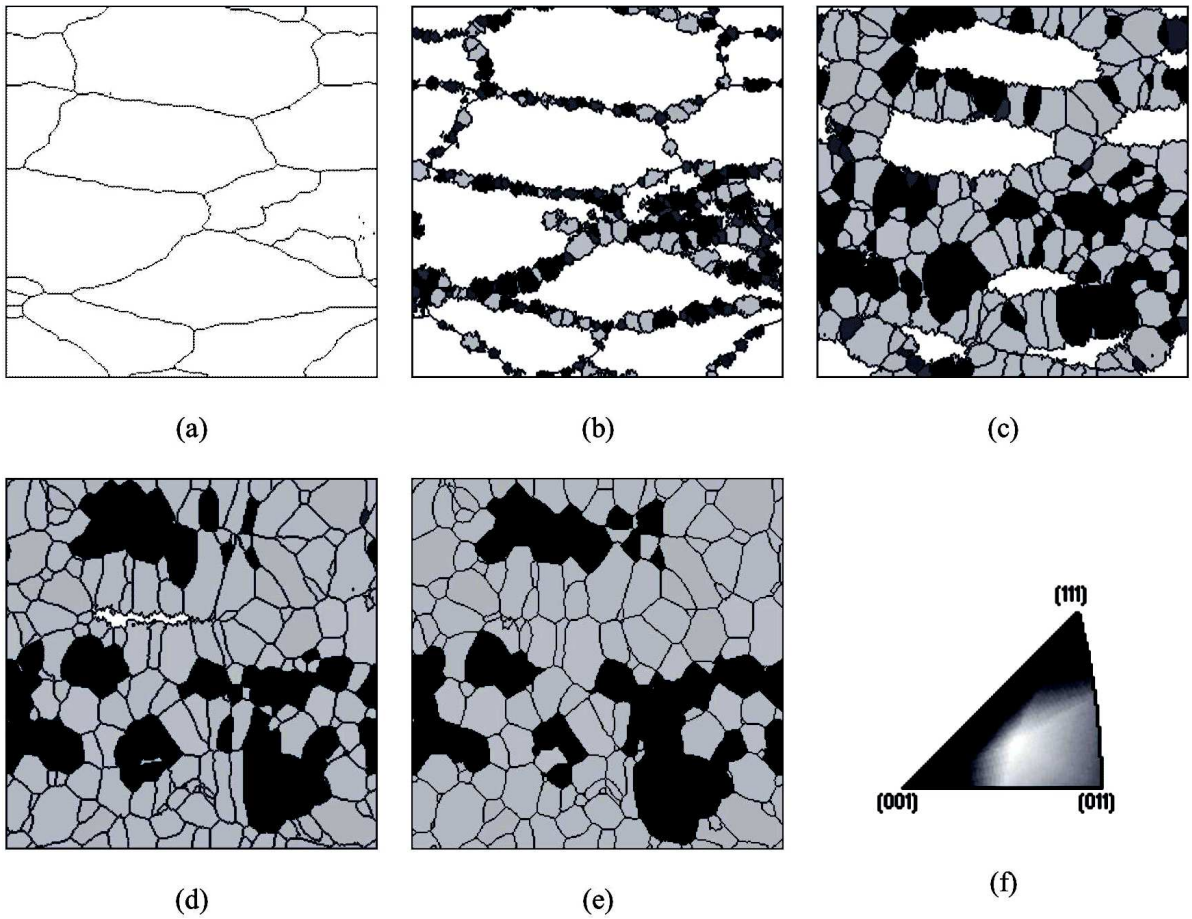

Fig. 2. MC-predicted microstructure evolution for Case 1 (RD-ND cross-section #125 of 250): (*a*) initial microstructure and microstructure after (*b*) 25, (*c*) 100, (*d*) 250, (*e*) 500 MCS, and (*f*) the grey scale key for the inverse-pole-figure map. (Only recrystallized grains are painted grey)

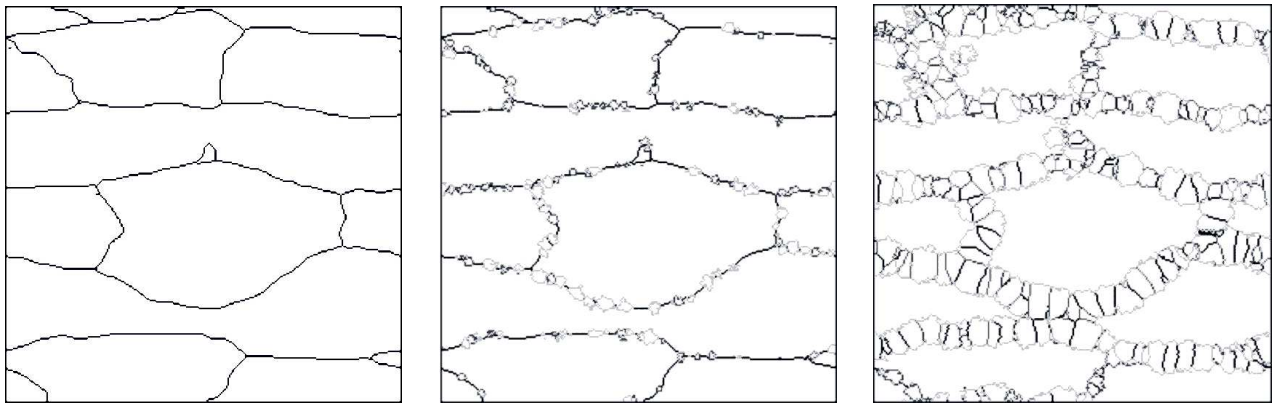

a **b** **c**

Fig. 3. MC-predicted microstructure evolution for Case 1 (ND-TD cross-section #125 of 250): (*a*) initial microstructure and microstructure after (*b*) 10 and (*c*) 40 MCS. The grain boundaries painted as bold have lowest effective mobility

misorientation. Therefore, the present approach takes into account the properties of special boundaries in an *average* sense only. Most Σ7 and Σ9 boundaries have a scalar misorientation between 25 and 37 degrees; hence, one can apply the effective mobility as shown in Fig. 1,*b* (Cases 1 and 2) for these GBs. Different probabilities for each type of nuclei were used, namely, P(Σ7) = 0.25, P(Σ9) = 0.25, and P(HABs) = 0.50.

Microstructure-evolution predictions for Case 1 and Case 2 were similar. Figure 2 summarizes these predictions for Case 1; different grain orientations are shown in the inverse-pole-figure map (Fig. 2,*f*). As expected, nuclei of different types exhibit different EM (Fig. 3,*a, b*), and the local speed of the recrystallization front was not constant.

3.2. Case 3 (reference case)

This simulation was run to provide a baseline for the effect of the properties of special boundaries on the recrystallization kinetics. The initial grain structure and the texture, as well as oriented-nucleation conditions, were assumed to be the same as for Cases 1 and 2. The effective grain-boundary mobility for special grain boundaries (Σ7 and Σ9) was assumed to be equal to that for arbitrary high-angle boundaries (Fig. 1,*b*), however.

Figure 4 summarizes the microstructure-evolution predictions for Case 3. The final grain size was found to be noticeably greater in comparison to that for Case 1. In addition, a large variety of texture components was developed in the final microstructure.

3.4. Recrystallization kinetics

Avrami plots were constructed and compared to quantify the overall recrystallization kinetics for the three different cases (Fig. 5). The predicted kinetics for Case 3 was found to be different from those for Cases 1 and 2. Because the nucleation rate was assumed to be the same in all cases, the similar kinetics predicted by the MC model for Cases 1 and 2 demonstrated that the effective mobility is indeed the principal factor controlling the kinetics.

It is also of interest to note that the kinetics for Cases 1 and 2 provided a better fit to the classical JMAK behavior. Nevertheless, it is unusual to find experimental data which show, on the detailed analysis, a good agreement with the JMAK behavior. Either the Avrami plot is not linear, or the slope is less than the expected value of 3, or both. For example, there are numerous investigations for aluminum and other materials, in which values of n of the order of 1 have been found [3]. The predicted Avrami exponents in the present work varied from 1.0 to 2.2. These predictions thus agree well with experimental data and modeling results in several previous investigations [3, 27, 30, 31], keeping in mind that the experimental slope usually reflects the JMAK kinetics only in the vicinity of a fraction recrystallized of 0.65 [32]. For the present modeling results, the predicted retardation of the recrystallization in comparison with the ideal JMAK kinetics after the recrystallized volume fraction reached ∼60-65% was probably a result of the discrete nature of the model domain as well as approximations concerning the mobility dependence on misorientation. Such an effect is typical in numerical simulations of recrystallization [30].

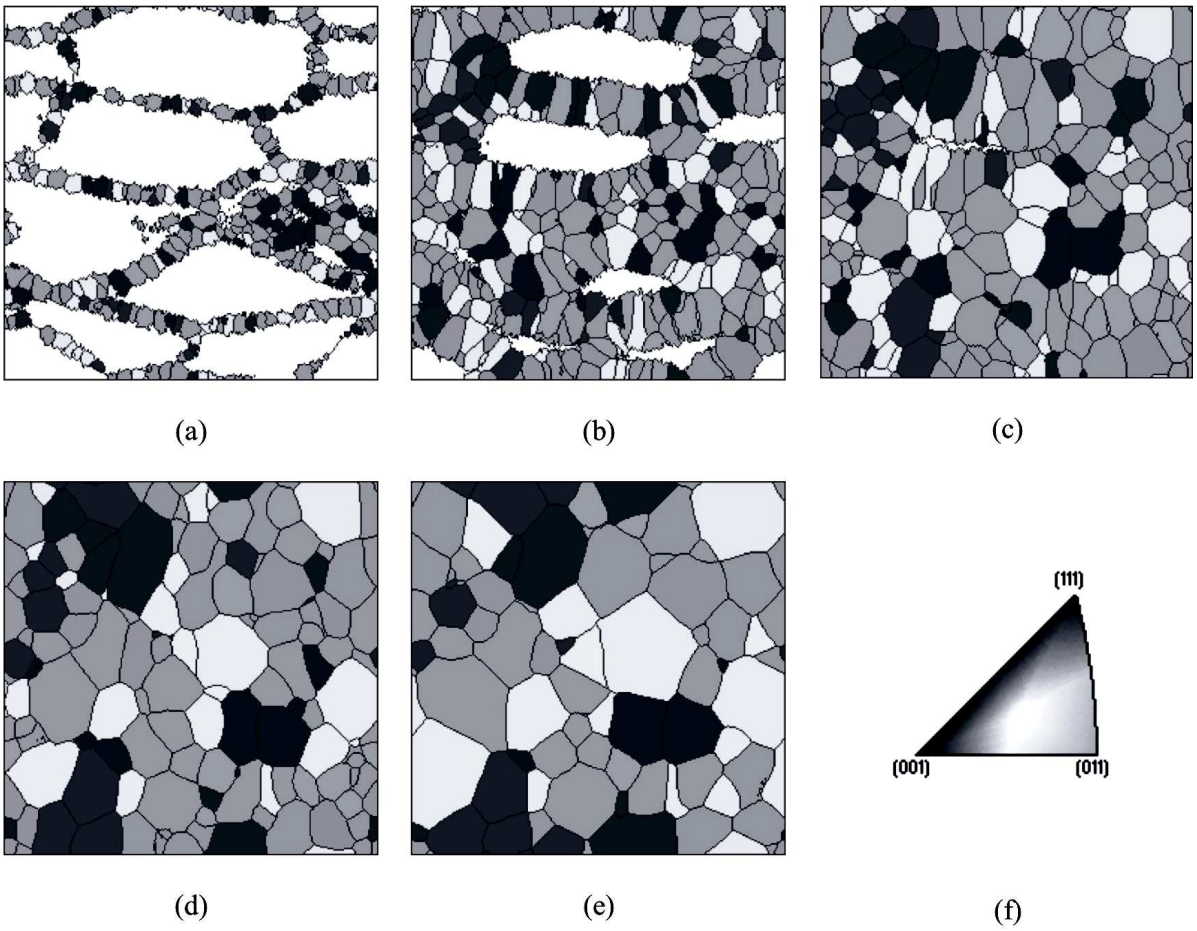

Fig. 4. MC-predicted microstructure evolution for Case 3 (RD-ND cross-section #125 of 250): microstructure after (*a*) 25, (*b*) 100, (*c*) 250, (*d*) 500, (*e*) 1000 MCS, and (*f*) the grey scale key for the inverse-pole-figure map. (Only recrystallized grains are painted grey)

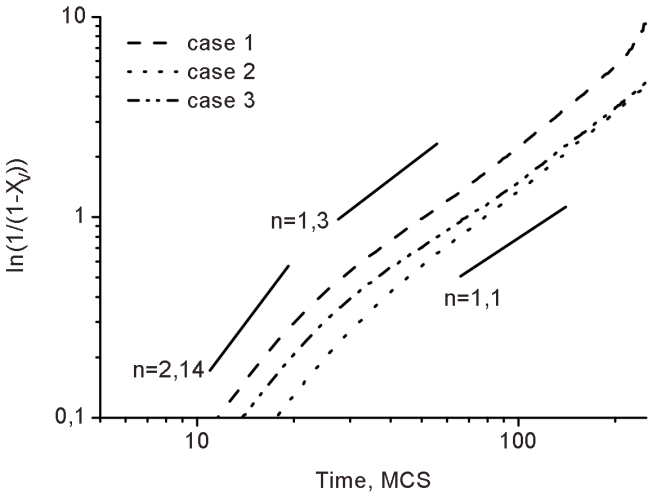

Fig. 5. Comparison of the MC-predicted recrystallization kinetics for Cases 1–3 (broken lines) and a fit based on the JMAK relation (solid lines)

3.5 Recrystallized grain-size distributions

MC predictions of the grain-size distribution (GSD) within the recrystallized modeling volume for Cases 1–3 at 20, 50, and 90% fraction recrystallized are summarized in Fig. 6,*a–c*. On the early stages of the recrystallization (∼20% recrystallized), the predicted GSDs for Cases 1 and 2 exhibited two maxima. The first one corresponds to grains surrounded mainly by general HABs, and the second one to grains surrounded by special GBs (Σ7 and Σ9). For all cases, the width of the GSD increased with the fraction recrystallized; however, this trend was less pronounced for Case 3.

The simulated GSDs are compared to the ideal log-normal distribution [33] in Fig. 6,*d*. This comparison reveals that the simulated GSD results are realistic with respect to the log-normal distribution usually found experimentally in recrystallized microstructures [3, 34].

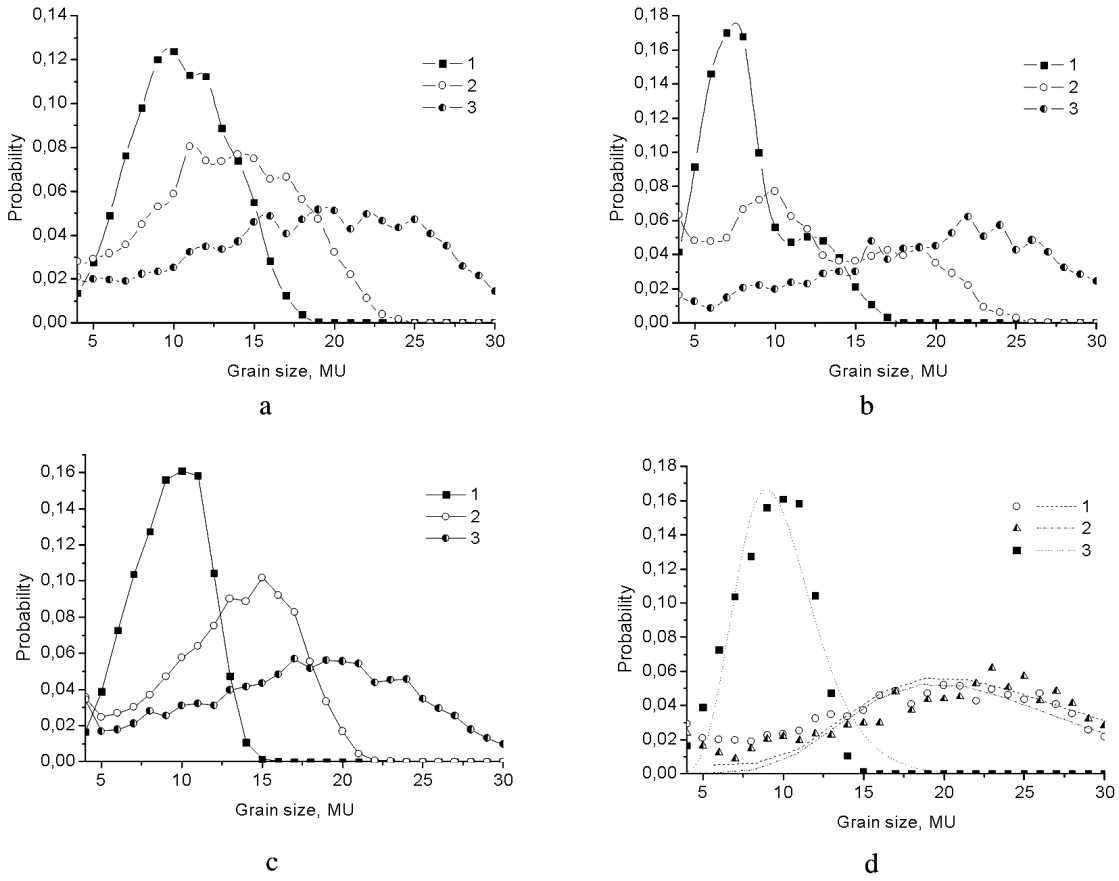

Fig. 6. MC-predicted grain-size distributions for (*a*) Case 1, (*b*) Case 2, and (*c*) Case 3 corresponding to recrystallized volume fractions of *1* – 20, *2* – 50, and *3* – 90%. The MC-predicted grain-size distributions are compared in (*d*) to classical log-normal distributions [3, 33]: *1* – Case 1, 90% recrystallized, *2* – Case 2, 90% recrystallized, and *3* – Case 3, 20% recrystallized

The evolution of the average grain size as a function of time is summarized in Fig. 7. These results reveal that differences in the EM for the three cases strongly affect the microstructure evolution. During the recrystallization, the average grain size for Cases 1 and 2 was predicted to grow two times faster than that for Case 3. However, immediately following the completion of the recrystallization (at ∼150 MCS), the grain growth for Cases 1 and 2 was noticeably slowed. This phenomenon can be rationalized as follows. Recrystallized nuclei develop on grain boundaries and grow toward the unrecrystallized areas. Nuclei surrounded mainly by GBs with high mobility (i.e., special CSL-type boundaries (Σ7 and Σ9) in Case 1 and general HABs in Case 2) grow much faster than nuclei surrounded only by GBs with intermediate mobility. The impingement of growing nuclei results in a rugged topography of the recrystallization front. The nonuniform growth of recrystallized grains results in the

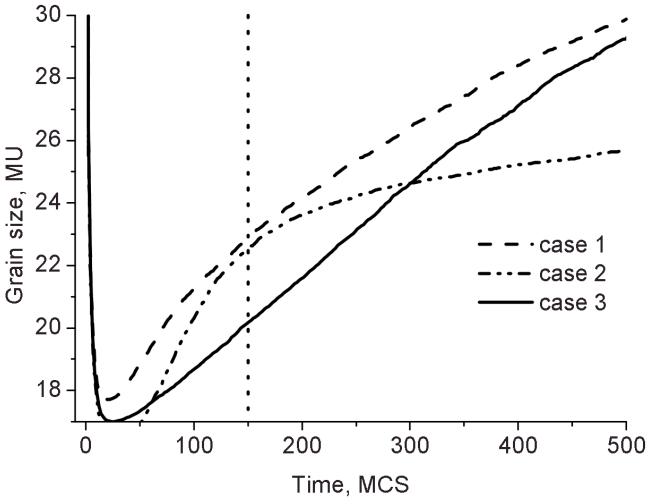

Fig. 7. MC-predicted average grain size evolution for Cases 1–3. The time interval from 0 to ∼ 150 MCS corresponds to recrystallization

formation of isolated unrecrystallized regions. Due to the subsequent disappearance of these isolated unrecrystallized regions, the surface area of the recrystallization front becomes lower, and a large fraction of low-angle grain boundaries are formed between the recrystallized grains. Hence, the rate of grain growth is retarded.

4. Summary and Conclusions

The recrystallization of polycrystalline metallic materials was modeled using a 3D Monte-Carlo (Potts) approach, in which the initial microstructure, texture (ODF), spatial distribution of the stored energy of deformation, nucleation mechanism, GB energy, and mobility were incorporated. Several simulations were performed to determine how the properties of CSL-type boundaries affect the recrystallization and the grain growth. The main conclusion is that special (CSL) type boundary properties have a marked effect on the final microstructure and the recrystallization kinetics. For instance, in the case where the EM of special CSL type grain boundaries is substantially lower than that for arbitrary HABs, the recrystallization rate is higher than that for the reference case without special boundary properties; in such an instance, a much smaller average grain size can be obtained after the grain growth following the recrystallization. It was also shown that the model predictions are in good agreement with the theoretical JMAK kinetics and yield realistic grain-size distributions for the recrystallized microstructure.

1. F. Haessner (Ed.), *Recrystallization of Metallic Materials* (Riederer, Stuttgart, 1978).
2. R.D. Doherty, D.A. Hughes, F.J. Humphreys, J.J. Jonas, D. Jul Jensen, M.E. Kassner, W.E. King, T.R. McNelly, H.J. McQueen, and A.D. Rollett, Mater. Sci. Eng. **A238**, 219 (1997).
3. F.J. Humphreys and M. Hatherly, *Recrystallization and Related Annealing Phenomena* (Elsevier, Oxford, 1995), pp. 85–126, 173–220.
4. D.J. Srolovitz, G. Grest, M.P. Anderson, and A.D. Rollett, Acta Metall. **34**, 1833 (1986).
5. V. Erukhimovitch and J. Baram, Mater. Sci. Eng. **A214**, 78 (1996).
6. R.L. Goetz and V. Seetharaman, Metall. and Mater. Trans. **29A**, 2307 (1998).
7. R.L. Goetz and V. Seetharaman, Scripta Mater. **38**, 405 (1998).
8. V. Marx, F.R. Reher, and G. Gottstein, Acta Mater. **47**, 1219 (1999).
9. B. Radhakrishnan, G.B. Sarma, and T. Zacharia, Acta Mater. **46**, 4415 (1998).
10. H.S. Zurob, C.R. Hutchinson, Y. Brechet, and G. Purdy, Acta Mater. **50**, 3075 (2002).
11. H.P. Stuwe, A.F. Padilha, and Jr.F. Siciliano, Mater. Sci. Eng. **A333**, 361 (2002).
12. R.W Cahn, in *Physical Metallurgy*, edited by R.W. Cahn and P. Haasen (Elsevier, Amsterdam, 1996), pp. 2400–2492.
13. F. Caleyo, T. Baudin, and R. Penelle, Scripta Mater. **46**, 829 (2002).
14. N. Rajmohan and J.A. Szpunar, Acta Mater. **48**, 3327 (2000).
15. O.M. Ivasishin, S.V. Shevchenko, N.L. Vasiliev, and S.L. Semiatin, Acta Mater. **51**, 1019 (2003).
16. O.M. Ivasishin, S.V. Shevchenko, N.L. Vasiliev, and S.L. Semiatin, Mater. Sci. Eng. **A443** 216 (2006).
17. O.M. Ivasishin, N.L. Vasiliev, S.V. Shevchenko, and S.L. Semiatin, Ukr. J. Phys. **50**, 1361 (2005).
18. H.J. Bunge, *Texture Analysis in Materials Science* (Butterworths, London, 1982).
19. H.J. Bunge, in *Quantitative Texture Analysis*, edited by H.J. Bunge and C. Esling (DGM-Informationsgesellschaft, Oberursel, 1981), p.1.
20. X. Song and M. Rettenmayr, Mater. Sci. Eng. **A332**, 153 (2002).
21. G. Zhu, W. Mao, and Y. Yu, Scripta Mater. **42**, 37 (2000).
22. M.G. Glavicic, P.A. Kobryn, T.R. Bieler, and S.L. Semiatin, Mater. Sci. Eng. **A346**, 50 (2003).
23. A.P. Sutton and R.W. Balluffi, in *Interfaces in Crystalline Materials* (Clarendon Press, Oxford, 1995).
24. M. Winning, G. Gottstein, and L.S. Shvindlerman, Acta Mater. **50**, 353 (2002).
25. D. Wolf, Acta Metall. Mater. **38**, 781 (1990).
26. P.G. Shewmon, in *Recrystalization, Grain Growth, and Textures* (ASM, Metals Park, OH, 1966), p.165.
27. G. Gottstein and L.S. Shvindlerman, in *Grain Boundary Mobility in Metals* (CRC Press, New York, 1999).
28. D. Weaire and S. McMurry, in *Solid State Physics: Advances in Research and Applications*, edited by M. Ehrenreich and F. Spaepen (Academic Press, San Diego, CA, 1996), p.1.
29. P. Gordon and R.A. Vandermeer, in *Recrystalization, Grain Growth, and Textures* (ASM, Metals Park, OH, 1966), p.205.
30. P. Uranga, A.I. Fernandez, B. Lopez, and J.M. Rodriguez-Ibabe, Mater. Sci. Eng. **A345**, 319 (2003).
31. A.D. Rollett, Progress in Mater. Sci. **42**, 79 (1997).
32. E. Valencia Morales, L.J. Vega, C.E. Villar, M.J. Antiquera, and R.C. Fadragas, Scripta Mater. **52**, 217 (2005).
33. S.K. Kurtz and F.M.A. Carpay, J. Appl, Phys. **51**, 5725 (1980).
34. T. Saetre, O. Hunderi, and E. Nes, Acta Metall. **34**, 981 (1986).

Received 22.12.06

ВПЛИВ МЕЖ КРИСТАЛІЧНИХ ЗЕРЕН СПЕЦІАЛЬНОЇ ГЕОМЕТРІЇ НА КІНЕТИКУ РЕКРИСТАЛІЗАЦІЇ ТА РОСТУ ЗЕРЕН

М.Л. Васильєв, С.В. Шевченко, О.М. Івасишин

Р е з ю м е

Досліджено вплив властивостей спеціальних меж зерен на процеси рекристалізації та росту кристалічного зерна при термічній обробці. Традиційно, моделючи процеси, використовували спрощені залежності рухливості та енергії межі зерна від скалярного розоріентування межі, а саме малокутові межі вважали такими, що мають меншу за інші межі зерен ефективну рухливість. У роботі проведено аналіз залежності кінетики рекристалізації у тривимірній моделі Монте-Карло з врахуванням відмінної рухливості і спеціальних меж зерен. Також запропоновано модифікації стандартної Монте-Карло-моделі Потса, які дозволяють починати процедуру моделювання з реалістичних вихідних мікроструктур та текстур.